



Mesoscale size-promoted targeted therapy for acute kidney injury through combined RONS scavenging and inflammation alleviation strategy

Xiaoqing Han^{a,b}, Luopeng Bi^a, Jiao Yan^b, Panpan Song^{b,c}, Yanjing Wang^{b,c}, Xingbo Wang^{b,c}, Yunyun Wu^d, Xiaobo Ding^e, Haiyuan Zhang^{b,c,*}, Yanbo Wang^{a,**}, Xi Li^{d,***}

^a Department of Urology, First Hospital of Jilin University, Changchun, 130021, China

^b Laboratory of Chemical Biology, Changchun Institute of Applied Chemistry, Chinese Academy of Sciences, Changchun, 130022, China

^c University of Science and Technology of China, Hefei, Anhui, 230026, China

^d School of Chemistry and Life Science, Changchun University of Technology, Changchun, 130012, China

^e Department of Radiology, First Hospital of Jilin University, Changchun, 130021, China

ARTICLE INFO

Keywords:

Mesoscale size
Acute kidney injury
Kidney targeting
Antioxidant stress
Inflammation alleviation

ABSTRACT

Acute kidney injury (AKI) is a heterogeneous, high-mortality clinical syndrome with diverse pathogenesis and prognosis, but it lacks the effective therapy clinically. Its pathogenesis is associated with production of reactive oxygen/nitrogen species and infiltration of inflammatory cells. To overcome these pathogenic factors and improve the therapeutic efficiency, we synthesized triptolide-loaded mesoscale polydopamine melanin-mimetic nanoparticles (MeNP₄^{TP}) as the antioxidant plus anti-inflammatory therapeutic platform to synergistically scavenge reactive oxygen/nitrogen species (RONS), inhibit the activity of macrophages and dendritic cells, and generate Treg cells for AKI therapy. It was demonstrated that mesoscale size was beneficial for MeNP₄^{TP} to specifically accumulate at renal tubule cells, and MeNP₄^{TP} could significantly attenuate oxidative stress, reduce proinflammatory immune cells in renal, and repair renal function in cisplatin-induced AKI mouse model. MeNP₄^{TP} might be a potential candidate to inhibit oxidative damages and inflammatory events in AKI.

1. Introduction

Acute kidney injury (AKI) is a heterogeneous, high-mortality clinical syndrome with diverse pathogenesis and prognosis [1]. AKI usually presents as renal insufficiency, resulting in the accumulation of metabolic wastes that disrupt water, electrolytes and acid-base dynamics [2]. Importantly, the most AKI will develop the chronic kidney disease and eventually lead to the kidney failure [3]. The clinical treatment of AKI mainly relies on kidney dialysis or kidney transplantation, both of which are expensive to treat, and the mortality rate is still unsatisfactory [4–6]. Therefore, the development of effective AKI treatments is necessary and urgently needed.

Oxidative stress plays an important role in the AKI pathogenesis [7]. The damaged kidney cells produce a large number of reactive oxygen/nitrogen species (RONS) to cause the oxidative stress [8], which can activate some cell signaling pathways, such as mitogen-activated protein

kinase (MAPK) and protein 53, leading to the renal tubular cell death [9]. Moreover, RONS also contribute to the renal fibrosis process by enhancing inflammation [9]. Elimination of excess RONS can protect the kidney tissue from oxidative stress. The administration of antioxidants (such as amifostine) has already been used to scavenge ROS in AKI [10]. However, the side effects limit its wider applications. Inflammation is a complex biological reaction of the body and also an important part of the pathophysiology of AKI [7]. The injured kidney cells release cytokines or chemokines to recruit immune cells to the site of kidney injury, forming a pro-inflammatory microenvironment [11]. Immune cells of the innate and adaptive immune systems, such as dendritic cells (DCs), macrophages, and T lymphocytes, contribute to the development of AKI by secreting pro-inflammatory factors, chemokines, and adhesion molecules that cause inflammation in the kidney [12,13]. For these reasons, inhibiting the function of pro-inflammatory immune cells has received much attention to regulate the inflammation following AKI. For

* Corresponding author. Laboratory of Chemical Biology, Changchun Institute of Applied Chemistry, Chinese Academy of Sciences, Changchun 130022, China. University of Science and Technology of China, Hefei, Anhui 230026, China.

** Corresponding author. Department of Urology, First Hospital of Jilin University, Changchun, 130021, China.

*** Corresponding author. School of Chemistry and Life Science, Changchun University of Technology, Changchun 130012, China.

E-mail addresses: zhangh@ciac.ac.cn (H. Zhang), wangyanb@jlu.edu.cn (Y. Wang), xli@ccut.edu.cn (X. Li).

<https://doi.org/10.1016/j.mtbio.2024.101002>

Received 30 November 2023; Received in revised form 13 February 2024; Accepted 13 February 2024

Available online 16 February 2024

2590-0064/© 2024 The Authors. Published by Elsevier Ltd. This is an open access article under the CC BY-NC-ND license (<http://creativecommons.org/licenses/by-nc-nd/4.0/>).

example, adoptive transfer of $\text{TCR}^+ \text{CD4}^- \text{CD8}^-$ (double negative) T cells can recover the kidney function and structural damage in cisplatin-induced AKI [14], and polydopamine-coated manganese ferrite nanoparticles have been used in the treatment of AKI by polarizing M1-type macrophages into M2-type macrophages [15]. However, since various immune cells in the kidney form a complex inflammatory

regulatory network [13], regulating the function of a single type of immune cells is insufficient for the treatment of kidney injury. Therefore, the development of combined therapeutic strategy to simultaneously clear RONS and regulate multiple immune cell function will be effective for treatment of AKI.

The kidney is one of the main filtering organs of the body, so

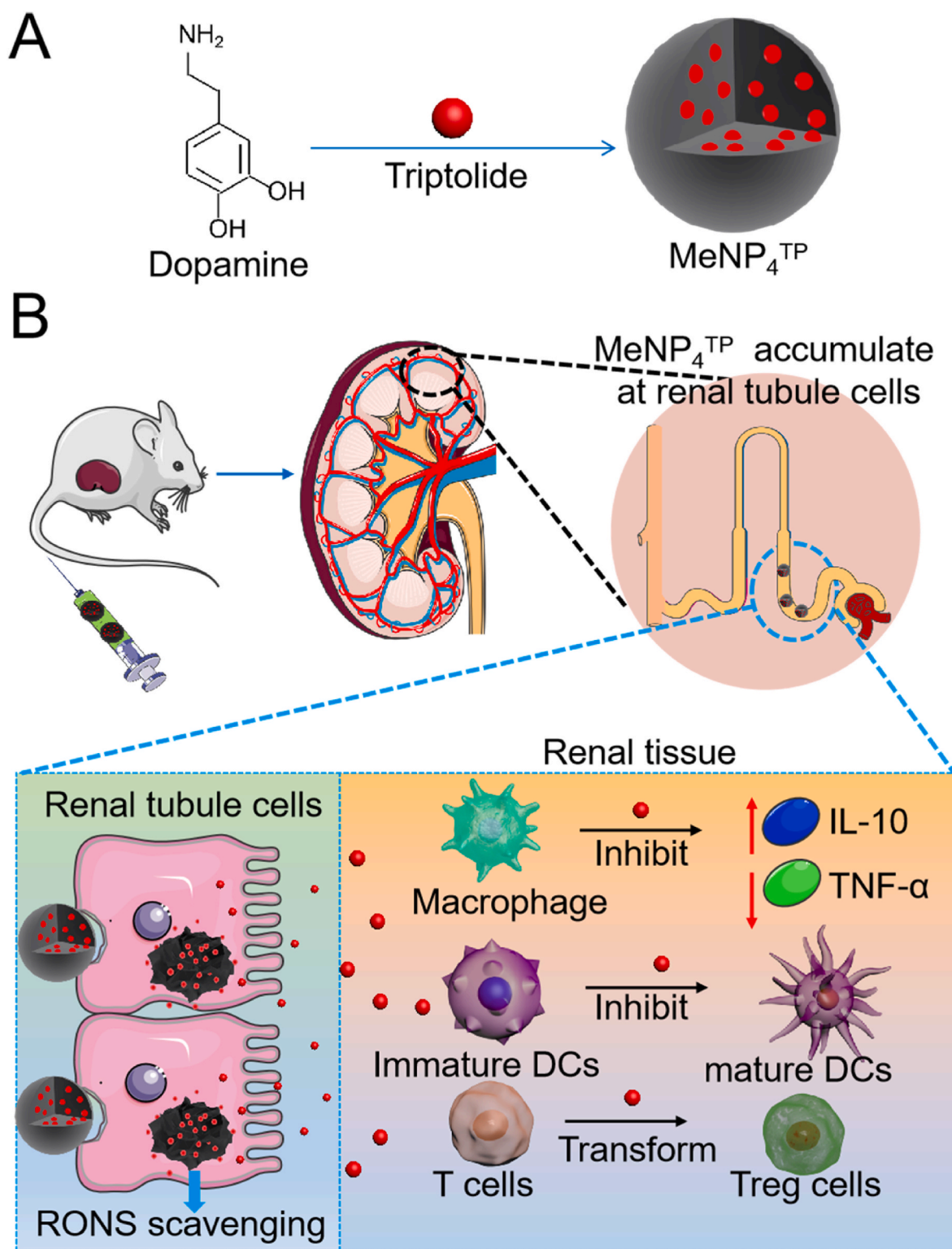


Fig. 1. Schematic illustration of synthesis and AKI therapeutic effects of MeNP₄^{TP}. (A) Synthesis process of MeNP₄^{TP}. (B) Therapeutic effect of MeNP₄^{TP} in AKI therapy. MeNP₄^{TP} specifically accumulated at renal tubule cells to remove intracellular RONS and repair the cell damage. TP was slowly released from MeNP₄^{TP} to inhibit the secretion of TNF- α , promote the secretion of IL-10 from macrophages, inhibit DCs mature, and increase the percentage of Treg cells in renal tissues.

nanoparticles have been attempted to naturally accumulate in the kidney to treat AKI. Although small size NPs (≤ 10 nm) can easily cross the glomerular filtration barrier and accumulate in the kidney, they will be quickly filtered out by the kidney, also resulting in low renal uptake [16–18]. Some studies have found that positively charged nanoparticles are cleared faster than neutral ones, followed by negatively charged nanoparticles, because nanoparticles with negative surface charge are more likely to be blocked by the renal filtration barrier [19,20]. However, the damage of the glomerular filtration membrane caused by AKI can destroy the surface charge of the renal filter barrier and reduces the renal accumulation of the nanoparticles [21]. The molecular recognition moieties that can bind to kidney cells, including antibodies, small molecules or aptamers, are being used to improve the kidney accumulation of nanocarriers [22]. However, most of these moieties are not specific to the kidney and the accumulation in other organs can cause the side effects. Even the renal tubular-targeting peptide-modified nanocarriers also have shown the enhanced drug distribution in the heart [23]. Recent studies found that mesoscale nanoparticles formed by polyethylene glycol (PEG)-coated poly(lactic-co-glycolic acid) (PLGA) polymer could specifically accumulate in the kidney through endocytosis of peritubular capillary endothelial cells after intravenous injection into the mice circulatory system [24]. This means that the mesoscale size of nanoparticles without surface modification can implement the kidney-targeting function. Therefore, the development of mesoscale drug formulation will be effective for targeted AKI therapy.

In the present study, triptolide (TP)-loaded mesoscale polydopamine nanoparticles (MeNP₄^{TP}) were designed for AKI therapy through an integrated strategy of inhibiting the pro-inflammatory immune cell function and clearing excessive RONS. Polydopamine nanoparticles (MeNPs) that possess various reductive functional groups (including catechol, amine and imine) [25,26] can efficiently capture RONS produced by AKI. The sizes of MeNPs were finely tuned to 200 nm (MeNP₂), 400 nm (MeNP₄) and 600 nm (MeNP₆), confirming the best kidney accumulation ability of MeNP₄ through a biodistribution study. TP, as an anti-inflammatory drug, inhibits the maturation and function of immune cells, such as macrophages, T cells and DCs [27–30]. Considering the poor water solubility, toxicity and low kidney-targeting ability of TP, polydopamine nanoparticles potentially can work as carriers for TP (Fig. 1A) based on the hydrogen bonding interaction between the C-14 hydroxyl group of TP and the catechol group of polydopamine, efficiently inhibiting the function of pro-inflammatory immune cells. The MeNP₄^{TP} was prepared by loading TP in MeNP₄ [31]. Through intravenous injection into cisplatin-induced AKI model mice, MeNP₄^{TP} could specifically accumulate at renal tubule cells based on their mesoscale size, efficiently scavenge RONS based on the antioxidant property of polydopamine, inhibit the activities of macrophages and DCs and promote the generation of Treg cells through release of TP (Fig. 1B). Therefore, MeNP₄^{TP} exhibited the significant therapeutic effect in AKI, holding the substantial potential for clinical use.

2. Results and discussion

2.1. Synthesis and characterization of MeNP₄^{TP}

The mesoscale MeNP₄ with a size of 400 nm were prepared through the oxidative self-polymerization of dopamine for 24 h in a mixed solution of water, ammonia, and ethanol at pH 10.8. For comparison, MeNP₂ and MeNP₆ with sizes of 200 and 600 nm, respectively, were similarly prepared through appropriate adjustment of pH condition. TEM images revealed that MeNP₂, MeNP₄ and MeNP₆ had primary sizes of 192.6 ± 5.9 , 393.3 ± 5.3 , and 591.3 ± 7.1 nm, and all of them showed monodispersed spherical morphology (Fig. 2A). Dynamic light scattering (DLS) analysis showed that MeNP₂, MeNP₄ and MeNP₆ had hydrodynamic sizes of 227.3 ± 5.4 , 425.6 ± 4.9 and 626.3 ± 9.9 nm, respectively (Fig. 2B). Zeta potential measurement indicated all these nanoparticles showed the negative surface charges in water (Fig. 2C).

Kidney-targeting ability of these nanoparticles was first investigated in AKI mouse model that was established through intraperitoneal injection of cisplatin in C57BL/6J mouse [32]. The 1,1'-dioctadecyltetramethylindotricarbocyanine iodide (DiR)-labeled MeNPs were injected intravenously into AKI mice at three days post-injection of cisplatin for the biodistribution assessment. At 24 h post-injection, major organs were collected for *ex vivo* imaging. Fig. 2D and E reveal that the mice treated with DiR-labeled MeNP₄ presented the most intense fluorescence intensity in kidneys among various nanoparticles, suggesting the significant accumulation of DiR-labeled MeNP₄ in the kidney. This result corroborates the kidney-targeting ability of MeNP₄.

Then, MeNP₄ was chosen as carrier to load TP, forming MeNP₄^{TP}. TEM image confirmed MeNP₄^{TP} still remained the mesoscale size of 397.6 ± 6.7 nm, hydrodynamic size of 425.0 ± 4.1 nm and negative surface charge of -29.9 ± 0.5 eV (Fig. 2A–C). The TP loading caused little effect on primary size, hydrodynamic size and morphology of MeNP₄ but weakened its negative surface charge. Considering the toxicity of TP, the loading capacity of TP in MeNP₄^{TP} was controlled to be 2.26%, as determined by high performance liquid chromatography (HPLC) analysis [33]. This loading capacity is beneficial for controlling the therapeutic dose and side effects of TP. The TP release profile of MeNP₄^{TP} was also investigated in phosphate buffered saline (PBS) solution containing 10% fetal bovine serum (FBS) by HPLC monitoring. MeNP₄^{TP} showed a sustained drug release behavior and the cumulative drug release reached the maximum value of 77.3 ± 1.2 % within 24 h (Fig. S1). Then, the free radical scavenging capacity of MeNP₄^{TP} was assessed by a 2,2-diphenyl-1-picrylhydrazyl (DPPH) method [25]. The result showed that MeNP₄^{TP} could effectively scavenge free radicals in a concentration-dependent manner, which was similar to the profile of MeNP₄ (Fig. S2). Furthermore, the scavenging capacities of MeNP₄^{TP} for hydroxyl radical, superoxide anion radical and peroxynitrite were also examined by terephthalic acid, pyrogallol and sodium nitrite (NaNO₂)/hydrogen peroxide (H₂O₂) assays, respectively. Similarly, both MeNP₄ and MeNP₄^{TP} showed significant scavenging abilities for these ROS/RNS (Fig. 2F–H).

2.2. *In vitro* oxidative stress injury protected by MeNP₄^{TP}

Excessive RONS can cause the oxidative stress and induce the cell damage [8]. Considering that renal tubules are vulnerable to the oxidative stress, human proximal tubular epithelial cells (HK-2 cells) were used to evaluate the protection ability of MeNP₄^{TP} against the oxidative stress. Before investigating the RONS elimination ability of MeNP₄^{TP} in cells, the biocompatibility of MeNP₄^{TP} in HK-2 cells and human umbilical vein endothelial cells (HUVEC) were evaluated using a 3-(4,5-dimethylthiazolyl-2)-2,5-diphenyltetrazolium bromide (MTT) assay. The results showed that MeNP₄ had little influence on the cell viability of HK-2 cells and HUVEC (Fig. S3A) and MeNP₄^{TP} showed the slight cytotoxicity against HK-2 cells and HUVEC at the highest concentration (Fig. S3B), while free TP exhibited severe cytotoxicity at the highest concentration (Fig. S3C). These results suggested that MeNP₄ significantly reduced the toxicity of TP due to the polydopamine encapsulation, excellent biocompatibility of polydopamine and slow release of TP from MeNP₄^{TP} [34].

Then, the cellular uptake of MeNP₄^{TP} and MeNP₄ was investigated in HK-2 cells by fluorescence microscopy and flow cytometry using rhodamine B (RhB)-labeled nanoparticles. After 3 h of incubation with RhB-labeled MeNP₄^{TP} and MeNP₄, the cells presented the potent fluorescence intensities (Fig. 3A and S4), which were much higher than that of cells incubated with free RhB, demonstrating that MeNP₄^{TP} and MeNP₄ can be efficiently taken up by HK-2 cells. Furthermore, the results of flow cytometry showed the similar trend (Fig. 3B). Then, the RONS elimination ability of MeNP₄^{TP} was investigated in HK-2 cells that were stimulated by cisplatin to induce

an oxidative stress injury [35]. Then, cisplatin-stimulated HK-2 cells were incubated with PBS, TP, MeNP₄ or MeNP₄^{TP} for 24 h, while

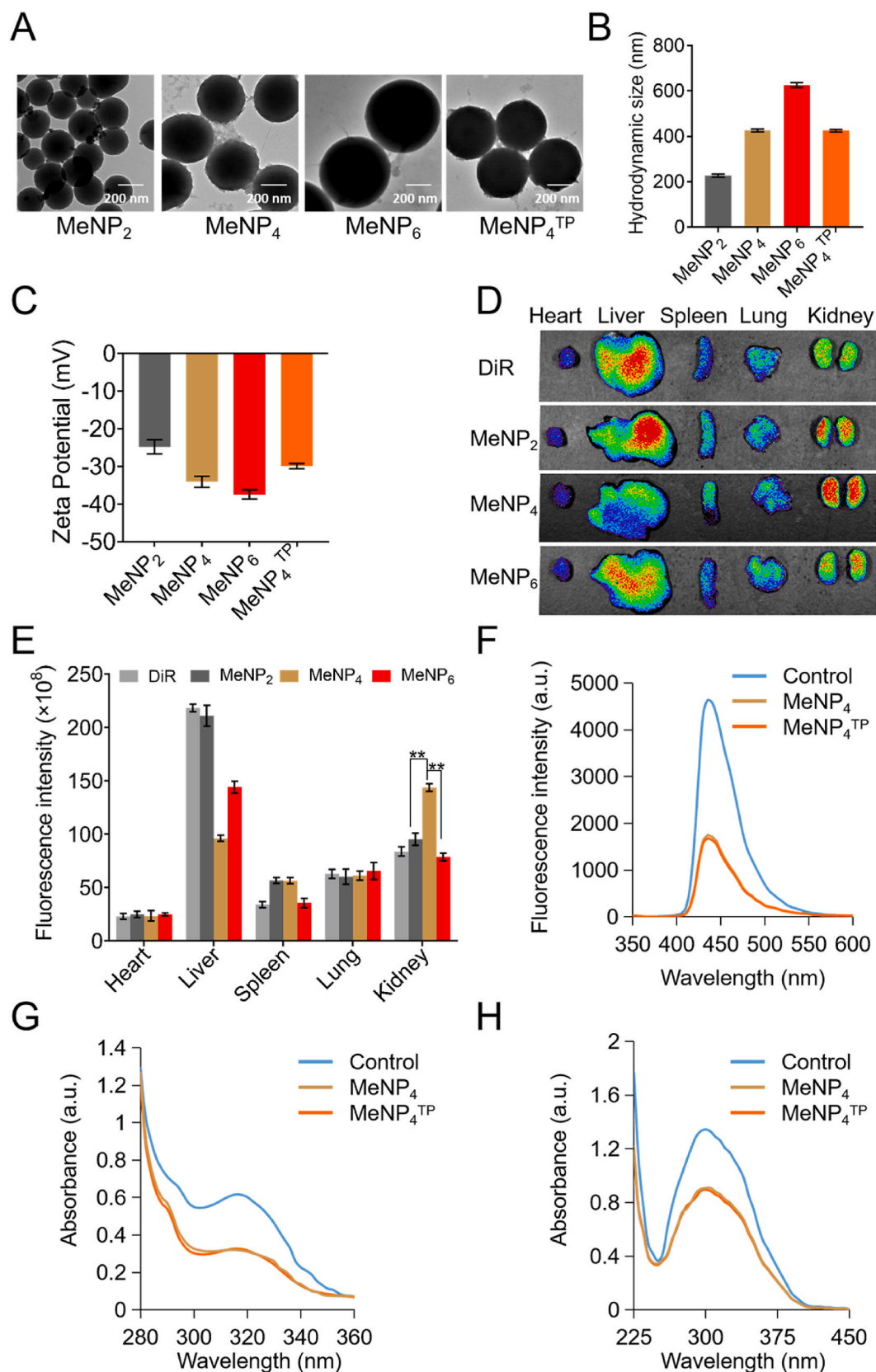


Fig. 2. Characterization of MeNP₄^{TP}. (A) TEM images of MeNP₂, MeNP₄, MeNP₆ and MeNP₄^{TP}. Scale bar, 200 nm. (B) Hydrodynamic sizes of MeNP₂, MeNP₄, MeNP₆ and MeNP₄^{TP}. (C) Zeta potential of MeNP₂, MeNP₄, MeNP₆ and MeNP₄^{TP}. (D) *Ex vivo* fluorescence images of major organs (heart, liver, spleen, lung and kidney) collected from mice treated with DiR-labeled MeNP₂, MeNP₄ or MeNP₆ at 24 h (0.05 mg kg⁻¹ mouse, according to DiR content). (E) Fluorescence intensity analysis in Fig. 2D (n = 5, **p < 0.01). (F) Hydroxyl radical scavenging capacity of MeNP₄ and MeNP₄^{TP}. The hydroxyl radical was produced by H₂O₂ under UV-irradiation. (G) Superoxide anion radical scavenging capacity of MeNP₄ and MeNP₄^{TP}. The superoxide anion radical was produced by the reaction of pyrogallol and oxygen at pH = 8.2. (H) Peroxynitrite radical scavenging capacity of MeNP₄ and MeNP₄^{TP}. The peroxynitrite radical was produced by the reaction between NaNO₂ and H₂O₂.

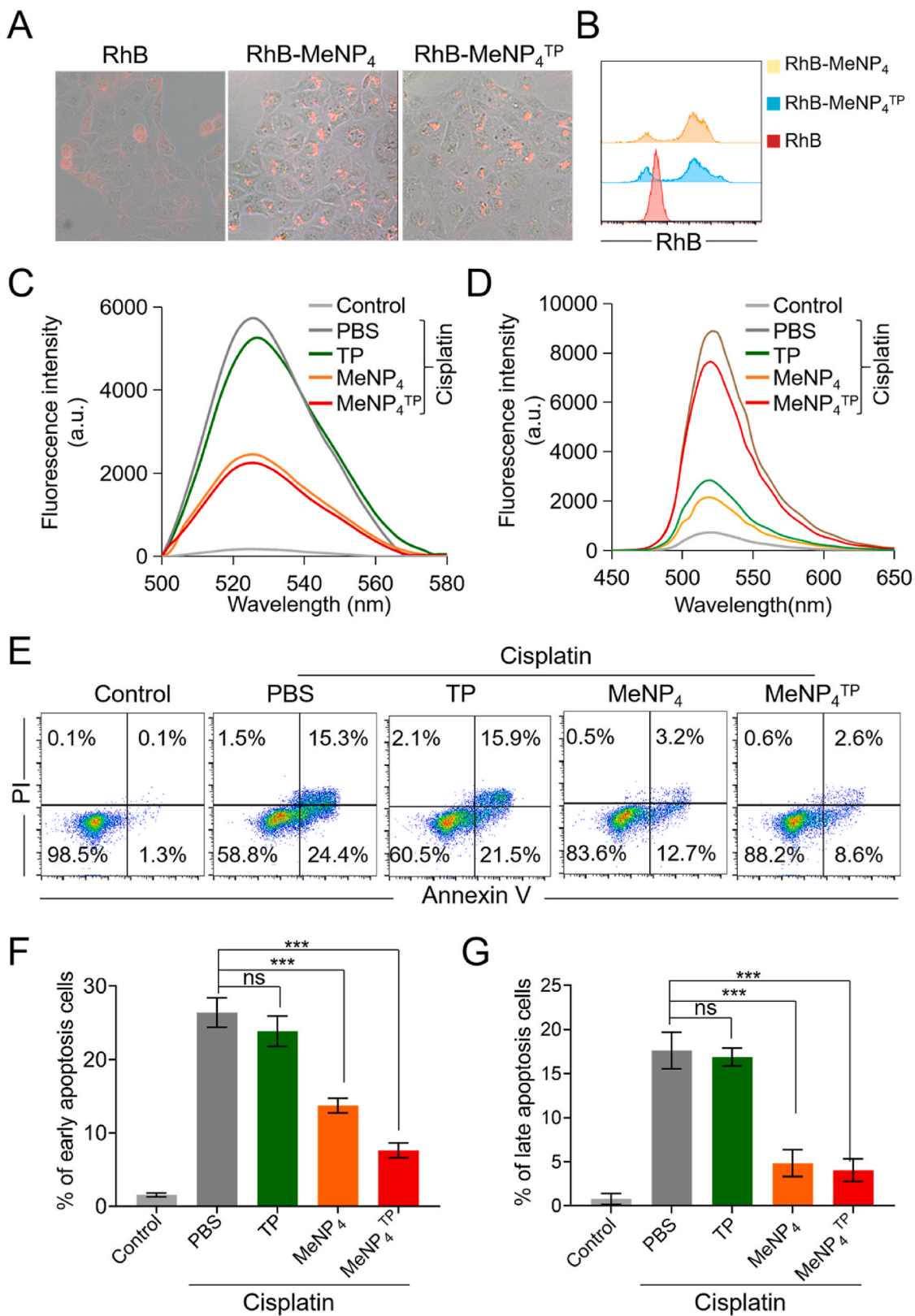


Fig. 3. MeNP₄^{TP} protected HK-2 cells from oxidative stress. (A, B) Fluorescent images (A) and flow cytometry analysis (B) of HK-2 cells treated with RhB, RhB-labeled MeNP₄^{TP}, and RhB-labeled MeNP₄ for 3 h. (C) DCF fluorescence emission spectra were collected at 500–580 nm with excitation at 488 nm for HK-2 cells treated with TP, MeNP₄ and MeNP₄^{TP} under cisplatin stimulation. (D) R21 fluorescence emission spectra were collected at 450–650 nm with excitation at 488 nm for HK-2 cells treated with TP, MeNP₄ and MeNP₄^{TP} under cisplatin stimulation. (E) Flow cytometry analysis for apoptotic HK-2 cells based on Annexin-FITC/PI assay after treatments with TP, MeNP₄ and MeNP₄^{TP} under cisplatin stimulation. (F) Quantification of early apoptotic HK-2 cells (FITC⁺ PI⁻) in Fig. 3E. (G) Quantification of late apoptotic HK-2 cells (FITC⁺ PI⁺) in Fig. 3E. Data are expressed as means ± SD (n = 3, ***p < 0.001; ns, not significant).

untreated cells served as control. The cellular ROS variation was evaluated by a fluorescence microplate reader using a 2',7'-dichlorodihydrofluorescein (DCF) fluorescent probe. Fig. 3C and S5A revealed that cells treated with PBS presented the high intracellular ROS level according to the intense DCF fluorescence, and the treatment with TP resulted in a slight decrease in DCF fluorescence intensity, suggesting the weak ROS reduction effect of TP. However, the treatment with MeNP₄^{TP} or MeNP₄ could dramatically reduce the DCF fluorescence intensity, demonstrating the efficient ROS scavenging capacity of MeNP₄^{TP} or MeNP₄. Next, the cellular RNS variation was evaluated by a fluorescence microplate reader using a R21 fluorescent probe. The result showed that the trend of RNS variation in different treatment groups was the same as that of ROS (Fig. 3D and S5B). Since excessive RONS can induce the cell apoptosis, the apoptosis profiles of HK-2 cells under various treatments were further examined by flow cytometry using a fluorescein isothiocyanate (FITC)-Annexin V/propidium iodide (PI) assay. The results showed that the percentages of apoptotic cells including early apoptosis and late apoptosis were slightly decreased after treatment with TP, but these percentages were significantly decreased after treatment with MeNP₄^{TP} or MeNP₄, where MeNP₄^{TP} showed the more inhibitory effect due to the combined RONS scavenging abilities of MeNP₄ and TP (Fig. 3E-G). Collectively, all above results demonstrate that MeNP₄^{TP} can scavenge the RONS and alleviate the apoptosis of HK-2 cells induced by cisplatin.

2.3. *In vitro* immunosuppression promoted by MeNP₄^{TP}

Innate and adaptive immune responses are involved in mediating tubular cell injury and recovery of AKI. Overactivation of all the macrophages, DCs and T lymphocytes contribute to kidney injury. In contrast, M2 macrophages, inhibitory DCs and Treg cells are critical in inhibiting inflammation, tissue remodeling, and repair after kidney injury [36]. To determine whether MeNP₄^{TP} can regulate immune cells function, the macrophage reprogramming ability of MeNP₄^{TP} was firstly evaluated in RAW 264.7 cells by flow cytometry using FITC-F4/80, PE-CD86 and APC-CD206 antibodies. RAW 264.7 cells were pretreated with lipopolysaccharide (LPS) for 24 h to obtain M1 phenotype, followed by treatment with TP, MeNP₄ or MeNP₄^{TP} for another 24 h. Fig. 4A and S6A show that LPS could induce the vast majority of RAW 264.7 cells into M1 phenotype in PBS group, which had much higher expression of CD86 than control group that was without LPS treatment. The expression of CD86 was decreased and the expression of CD206 was increased in RAW 264.7 cells after treatment with TP, MeNP₄ or MeNP₄^{TP}, where MeNP₄^{TP} was more effective than TP and MeNP₄ (Fig. 4A and S6). To further demonstrate the role of MeNP₄^{TP} in inhibiting macrophages to acquire a pro-inflammatory phenotype, TNF- α (typical M1-type cytokine) and IL-10 (typical M2-type cytokine) secretions from the treated macrophages were also assessed by enzyme-linked immunosorbent assay (ELISA). As shown in Fig. 4B and C, all the treatments with TP, MeNP₄ and MeNP₄^{TP} could induce the higher levels of TNF- α and lower levels of IL-10 compared with those of PBS, where MeNP₄^{TP} exhibited more potent repolarization ability than others, consistent with the results of flow cytometry. All above results demonstrate that MeNP₄^{TP} can transform macrophages from a proinflammatory M1 phenotype to an anti-inflammatory M2 phenotype.

Immature DCs contribute to immune tolerance, however, mature DCs induce immune activation [37]. Then, the effect of MeNP₄^{TP} on DCs maturation was assessed through examining the expression of CD80 and CD86 which were the markers of DCs maturation by flow cytometry. Immature DCs separated from the bone marrow cells of normal C57BL/6J mice were incubated with LPS for 24 h to induce the cells maturation and further incubated with TP, MeNP₄ or MeNP₄^{TP} for another 24 h. The treatment with LPS could increase the CD80 and CD86 levels in DCs, indicating DCs maturation. After the treatments with TP, MeNP₄ or MeNP₄^{TP}, the levels of CD80 and CD86 were significantly decreased, where the treatment with MeNP₄^{TP} induced the lowest levels

(Fig. 4D and S7), demonstrating that MeNP₄^{TP} has excellent ability to inhibit DCs maturation in an inflammatory microenvironment.

Treg cells (CD4⁺ FOXP3⁺) that make up one subset of CD4⁺ lymphocytes suppress immunologic damage in AKI [38]. Thus, the effect of MeNP₄^{TP} on T cells activation was also detected. The spleen cells of C57BL/6J mice were treated with TP, MeNP₄ or MeNP₄^{TP} in the presence of CD3/CD28 for 48 h. Then, the percentage of Treg cells in CD4⁺ lymphocytes was analyzed by flow cytometry using PE-CD4 and FITC-FOXP3 antibodies. Fig. 4E and S8A show that there was no noticeable change in the percentage of total CD4⁺ lymphocytes, but the percentages of Treg cells were obviously increased in TP, MeNP₄ and MeNP₄^{TP} groups, and MeNP₄^{TP} still showed the largest increase (Fig. 4E and S8B). The above results confirm that MeNP₄^{TP} promoted immunosuppression *in vitro*, which is probably because TP can inhibit immune cells to acquire a pro-inflammatory phenotype and polydopamine nanoparticles can scavenge RONS to decrease pro-inflammatory stimuli.

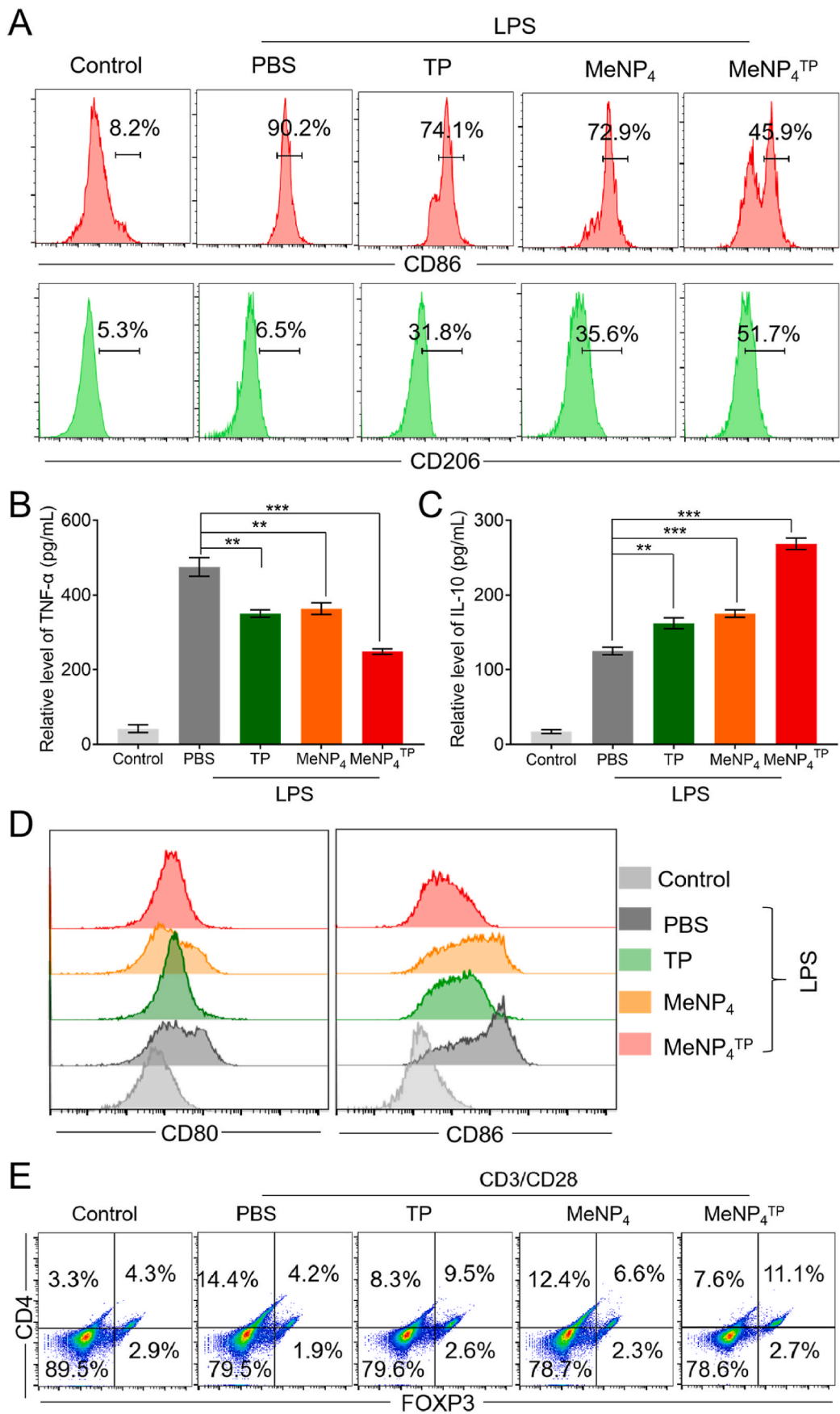
2.4. Therapeutic efficacy of MeNP₄^{TP} against cisplatin-induced AKI

Encouraged by above *in vitro* results, the *in vivo* therapeutic efficacy of MeNP₄^{TP} was then taken further investigation. To determine whether MeNP₄^{TP} can restore the renal function, the cisplatin-induced AKI mice were intravenously injected with PBS, TP, MeNP₄ or MeNP₄^{TP} for 3 consecutive days, respectively. After treatments, kidneys were collected from each group and sectioned for hematoxylin and eosin (H&E) staining. The result revealed that severe tubular dilation, tubular necrosis, cast formation and inflammatory cell infiltration were observed in PBS group (Fig. 5A). However, after the treatment with TP, MeNP₄ or MeNP₄^{TP}, these pathological responses were decreased, where MeNP₄^{TP} group could more remarkably decrease the pathological responses than TP and MeNP₄, which is ascribed to the abilities of promoting immunosuppression and scavenging RONS (Fig. 5A). Moreover, the levels of serum creatinine (CREA) and blood urea nitrogen (BUN), the key indicators of kidney function, were assessed in each group. Fig. 5B and C showed that the treatment with TP, MeNP₄ or MeNP₄^{TP} decreased CREA and BUN levels compared with PBS group, where the treatment with MeNP₄^{TP} exhibited the most potent effect among all these groups. Kidney injury molecule-1 (Kim-1) and neutrophil gelatinase-associated lipocalin (Ngal) are the important biomarkers of AKI [39]. Similar results were also achieved that the treatment with MeNP₄^{TP} induced the lowest

levels of Kim-1 and Ngal in the serum and urine of AKI mice (Figs. S9A–D), further confirmed the therapeutic effect of MeNP₄^{TP} against cisplatin-induced AKI. Cisplatin can also cause weight loss in mice. As showed in Fig. 5D, the body weights of AKI mice in PBS group were severely reduced when compared with the healthy mice, however, the treatment with TP, MeNP₄ or MeNP₄^{TP} alleviated the reduction in the body weight, and the body weight in MeNP₄^{TP} group showed the least reduction. Consistently, the survival analysis showed that the MeNP₄^{TP} group displayed the highest survival rate (80%), while the survival rate of PBS, TP and MeNP₄ group was 20, 30 and 50% at day 10, respectively (Fig. S10). The above results demonstrate the potential of MeNP₄^{TP} in restoring the renal function in AKI mice. The major organs (heart, liver, spleen and lung) were sliced and stained with H&E for histology analysis after different treatments. The results in Fig. S11 showed that there was no noticeable tissue damage in any of the main organs of different mice groups, indicating that MeNP₄^{TP} did not cause the obvious toxicity.

2.5. RONS scavenging and inflammation alleviation in the kidney by MeNP₄^{TP}

Oxidative stress and pro-inflammatory immune cell infiltration play important roles in the AKI pathogenesis. After the treatment, the level of RONS and the change in inflammatory cell phenotypes in the kidneys of AKI mice were further examined, respectively. Firstly, the ROS production in the kidneys were examined using a DCF probe. Compared with healthy mice, the ROS levels in the kidney of PBS-treated AKI mice



(caption on next page)

Fig. 4. MeNP₄^{TP} promotes the immunosuppression *in vitro*. (A) Flow cytometry analysis for the expression of CD86 and CD206 in RAW 264.7 cells. The cells were pretreated with LPS (100 ng mL⁻¹) for 24 h, then treated with TP, MeNP₄ or MeNP₄^{TP} (equivalent to 20 ng mL⁻¹ TP or 1 μg mL⁻¹ MeNP₄) for another 24 h and then stained with CD86-PE and CD206-APC antibodies. (B, C) ELISA analysis of the level of TNF-α (B) or IL-10 (C) in the medium as described in Fig. 4A. (D) Flow cytometry analysis for DCs maturation. The cells were pretreated with LPS (100 ng/mL) for 24 h, and then treated with TP, MeNP₄ or MeNP₄^{TP} (equivalent to 20 ng mL⁻¹ TP or 1 μg mL⁻¹ MeNP₄) for another 24 h, followed by staining with CD80-FITC and CD86-PE antibodies. (E) Flow cytometry analysis for the percentage of Treg cells. The cells were incubated with CD3/CD28 (5 μg mL⁻¹) and TP, MeNP₄ or MeNP₄^{TP} (equivalent to 20 ng mL⁻¹ TP or 1 μg mL⁻¹ MeNP₄) for 48 h, and then stained with CD4-PE and FOXP3-FITC antibodies. Data are expressed as means ± SD (n = 3, **p < 0.01, ***p < 0.001).

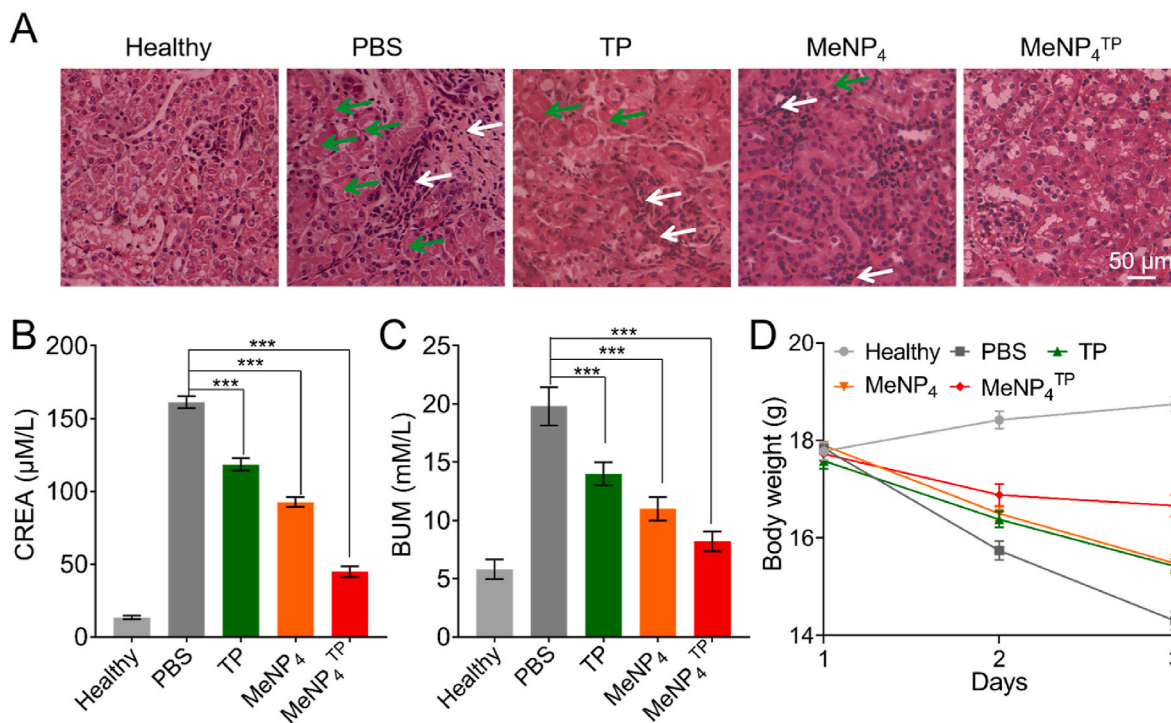


Fig. 5. Therapeutic efficacy of MeNP₄^{TP} against AKI mice. (A) H&E staining of the kidneys of different treatment groups. The green arrow indicates the tubular dilation, tubular necrosis, and cast formation. The red arrow indicates the inflammatory cell infiltration. Scale bar, 50 μm. (B–C) Levels of CREA (B) and BUN (C) of different treatment groups. (D) Body weight of different treatment groups. For Fig. 5A–D, The AKI mice were intravenously injected with PBS, TP, MeNP₄ or MeNP₄^{TP} (equivalent to 0.01 mg kg⁻¹ TP or 0.5 mg kg⁻¹ MeNP₄) for consecutive 3 days, respectively. Data are expressed as means ± SD (n = 5, ***p < 0.001). (For interpretation of the references to color in this figure legend, the reader is referred to the Web version of this article.)

were dramatically increased. For TP-, MeNP₄- or MeNP₄^{TP}-treated mice, the ROS levels in kidneys were gradually reduced, where the treatment with MeNP₄^{TP} resulted the largest reduction (Fig. 6A and S12A). Simultaneously, the RNS levels of the kidneys in different groups were examined using a O52 probes, showing the similar trend occurring in RNS levels (Fig. 6B and S12B). These results suggest that MeNP₄^{TP} could effectively scavenge free radicals in the kidney of AKI mice. Furthermore, the changes in inflammatory cell phenotypes including macrophages, DCs and CD4⁺ T cells in the kidneys of the treated mice were analyzed by flow cytometry. The percentages of M1 type macrophages (F4/80⁺ CD86⁺) and mature DCs (CD80⁺ CD86⁺) in the kidneys were decreased (Fig. 6C and D, S13A and S13B) and the percentage of M2 type macrophages (F4/80⁺ CD206⁺) was increased in TP, MeNP₄ and MeNP₄^{TP}-treated mice compared with that of PBS-treated mice, and the decrease induced by MeNP₄^{TP} was the most significant (Fig. 6C and S13C). Moreover, there was no significant variation in the percentage of CD4⁺ T cells in the kidneys of mice treated with TP, MeNP₄ or MeNP₄^{TP} compared with those treated with PBS, however, the percentage of Treg cells in CD4⁺ T cells was increased after treatment with TP, MeNP₄ or MeNP₄^{TP}, where the treatment with MeNP₄^{TP} led to the most increase (Fig. 6E and S14). All the above results confirm that MeNP₄^{TP} inhibited the accumulation of proinflammatory cells and promoted the recruitment of anti-inflammatory cells in the kidneys of AKI mice. Furthermore, the inflammatory factor levels including IFN-γ, IL-1β, TNF-α and IL-10 in the serum of the mice were detected by ELISA. The results

showed that MeNP₄^{TP} had the best performance in decreasing IFN-γ, IL-1β and TNF-α levels and increasing IL-10 level (Figs. S15A–D). The result indicated that the kidney microenvironment was in immunosuppressive state after the treatment of MeNP₄^{TP}. Therefore, MeNP₄^{TP} could treat AKI through modifying the inflammatory microenvironment of kidney injury by RONS scavenging and inflammation alleviation in the kidney.

3. Conclusion

In summary, we successfully prepared MeNP₄^{TP} as the antioxidant plus anti-inflammatory therapeutic formulations to modulate the inflammatory microenvironment of the kidney for AKI therapy. In AKI mice model, MeNP₄^{TP} exhibited the significant accumulation at the kidney due to their mesoscale size, and decreased the oxidative damage based on the ROS/RNS scavenging property of MeNPs, and their released TP modulated the renal microenvironment into an immunosuppressive state by inhibiting the accumulation of proinflammatory macrophages and mature DCs as well as increasing the proportion of Treg cells, which were beneficial for attenuation of AKI. These results revealed the potential of MeNP₄^{TP} for AKI therapy.

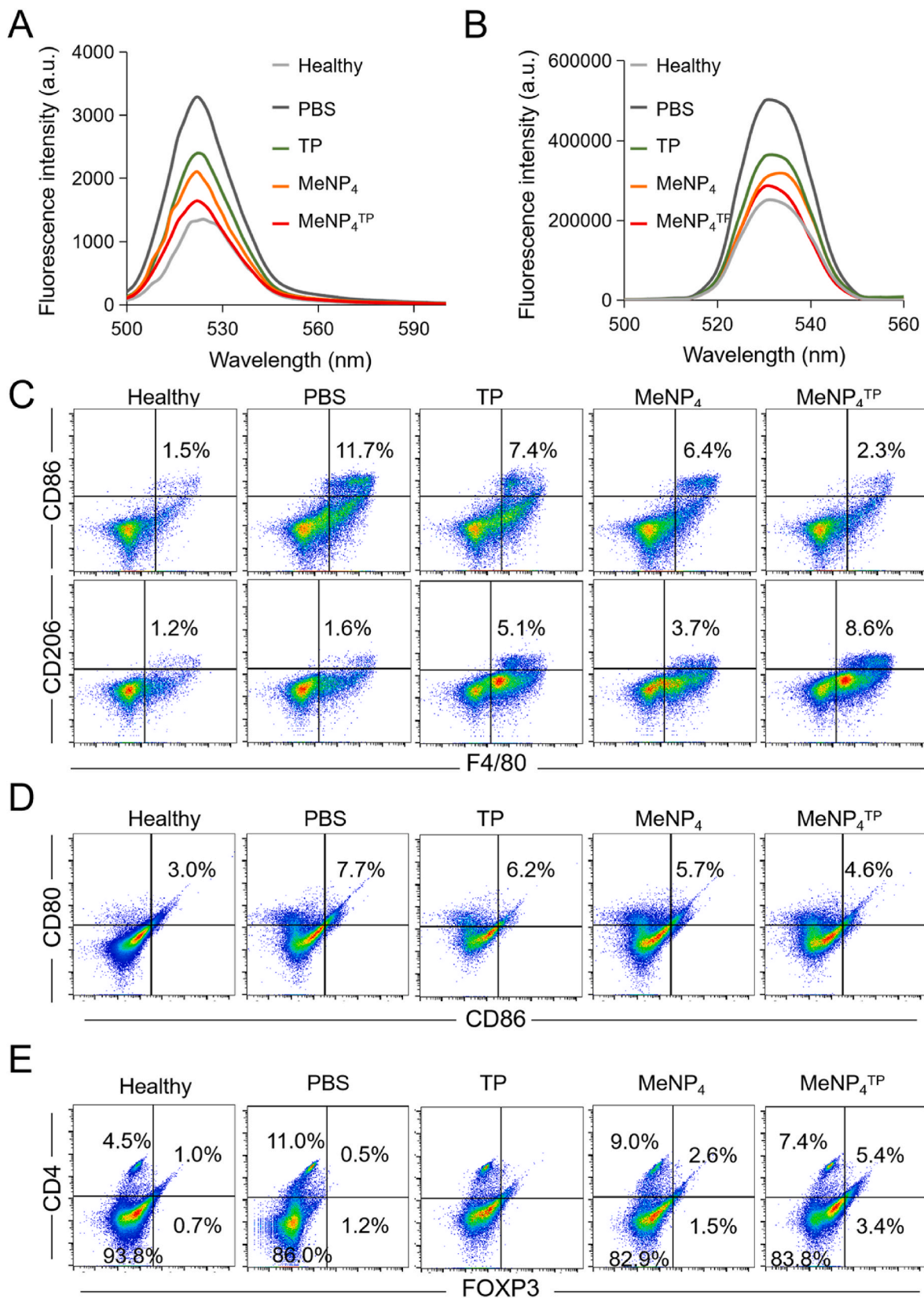


Fig. 6. RONS scavenging and inflammation alleviation in the kidney of AKI mice by MeNP₄^{TP}. (A) Fluorescence emission spectra were collected at 500–600 nm with excitation at 495 nm for ROS analysis based on DCF assay. (B) Fluorescence emission spectra were collected at 450–650 nm with excitation at 488 nm for RNS analysis based on O52 assay. (C) Flow cytometry analysis for the percentages of M1 and M2 type macrophages by staining with F4/80-FITC, CD86-PE and APC-CD206 antibodies. (D) Flow cytometry analysis for the percentage of mature DCs by staining with CD80-FITC and CD86-PE antibodies. (E) Flow cytometry analysis for the percentage of CD4⁺ T cells and Treg cells by staining with CD4-PE and FOXP3-FITC antibodies. For Fig. 6A–E, AKI mice were intravenously injected with PBS, TP, MeNP₄ or MeNP₄^{TP} (equivalent to 0.01 mg kg⁻¹ TP or 0.5 mg kg⁻¹ MeNP₄) for consecutive 3 days, respectively. Data are expressed as means ± SD (n = 5).

4. Materials and methods

4.1. Materials

Dopamine hydrochloride, 2,2 diphenyl-1-picryl hydrazyl (DPPH), TP and ammonium hydroxide were obtained from Sigma-Aldrich Corp (St. Louis, MO, USA). DiR, NaNO₂, hydrochloric acid (HCl), sodium hydroxide (NaOH), H₂O₂, terephthalic acid, tri(hydroxymethyl) amino methane hydrochloride (Tris-HCl), anionic surfactant sodium dodecyl sulfate (SDS), ethylenediaminetetraacetic acid disodium salt (Na₂EDTA), pyrogallol, 3-(4,5-Dimethylthiazol-2-yl)-2,5-diphenyltetrazolium bromide (MTT) and dimethyl sulfoxide (DMSO) were obtained from Aladdin Co. Ltd. (Shanghai, China). PI and Annexin-FITC assay kit were acquired from Yuanye Bio-Technology (Shanghai, China).

4.2. Synthesis of MeNP₄, MeNP₄^{TP} and DiR-labeled MeNP₂, MeNP₄ and MeNP₆

MeNP₄ were synthesized following the previous method with slight modification [25]. Briefly, 1 mL of ammonium hydroxide (28–30%) was added to a mixed solution containing 40 mL of ethanol and 90 mL of ultrapure water. The solution was magnetically stirred at room temperature for 30 min. 0.5 g of dopamine hydrochloride in 10 mL ultrapure water was dropwise added into the above solution. The solution was magnetically stirred for another 24 h MeNP₄ were collected by centrifugation and purified three times with ultrapure water. To synthesize MeNP₄^{TP}, the similar process was performed except adding 1 mg TP during the addition of dopamine hydrochloride. To synthesize MeNP₂ and MeNP₆, the similar process was performed except the volume of ammonium hydroxide (28–30%) was adjusted to 2 and 0.5 mL, respectively. To synthesize DiR-labeled MeNP₂, MeNP₄ and MeNP₆, the similar process was performed except 8.4 mg of DiR in 5 mL ethanol was added after addition of dopamine hydrochloride.

4.3. Characterization of MeNPs

Surface charge and hydrodynamic size of different MeNPs were determined by dynamic light scattering Malvern Zetasizer (Nano ZS, Malvern, USA). TEM image of different MeNPs were captured by transmission electron microscope (JEM-2010) with 200 kV of accelerating voltage. The UV-Vis absorption spectra of different MeNPs were measured by a Shimadzu UV-3600 spectrophotometer. The fluorescence spectra of different MeNPs were measured by a fluorescence microplate reader (BioTek Instruments, USA).

4.4. ROS and RNS scavenging analysis

The free radical scavenging capacity was analyzed by DPPH method [25]. The test was carried out in a 96 well plate using a total volume of 200 μ L of methanol containing 0.02 μ g mL⁻¹ DPPH and 0, 6.25, 12.5, 25, 50 or 100 μ g mL⁻¹ MeNP₄ or MeNP₄^{TP} for 30 min. Then, the absorbance at 520 nm was read by a Shimadzu UV-3600 spectrophotometer. Radical scavenging % of a certain concentration = (1 - Ax/A)*100%, where A is the absorbance at 520 nm of 0 μ g mL⁻¹ and Ax is the absorbance of 520 nm at a certain concentration.

For hydroxyl radical scavenging analysis, hydroxyl radicals were produced by 200 μ L of ultrapure water containing 5 mM H₂O₂ and 10 mM FeCl₃ under UV-irradiation of 5 min. 200 μ L of the resulting solution was mixed with 150 μ L of terephthalic acid (625 μ M), and added 50 μ L of MeNP₄ (200 μ g mL⁻¹), MeNP₄^{TP} (200 μ g mL⁻¹) or 50 μ L of deionized water (as control) in the dark at 37 °C for 1 h. Terephthalic acid was employed to trap the hydroxyl radical and generate 2-hydroxyterephthalic acid, quantifiable via fluorescence. The fluorescence spectrum of the resulting solution was then examined by a fluorescence microplate reader (BioTek Instruments, USA, Ex = 315 nm), in which the intensities were proportional to the hydroxyl radical levels in solution.

For superoxide radical scavenging analysis, 50 μ L of MeNP₄ or MeNP₄^{TP} (1.5 mg mL⁻¹) or 50 μ L of deionized water (as control) was mixed with 2900 μ L of Tris-HCl buffer (0.05 M, pH 8.2, 37 °C) containing 1 mM Na₂EDTA and added 50 μ L of pyrogallol (60 mM, 37 °C). Then, the mixed solution was shaken at 37 °C for 30 min. The UV absorption spectrum from 280 to 400 nm was read by a Shimadzu UV-3600 spectrophotometer.

For peroxynitrite scavenging analysis, NaNO₂ (10 mL, 50 mM) and H₂O₂ (10 mL, 50 mM) were mixed in ice water bath under quick stirring. Then, HCl (5 mL, 1 M) and NaOH (5 mL, 1.5 mM) were added into the mixture under the stirring, respectively. 10 μ L of the resulting solution was mixed with 90 μ L of deionized water and 20 μ L of MeNP₄ or MeNP₄^{TP} (150 μ g mL⁻¹) or 20 μ L of deionized water (as control) for 30 min. The UV absorption spectrum from 250 to 450 nm was read by a Shimadzu UV-3600 spectrophotometer.

4.5. TP release analysis

The release profile of TP from MeNP₄^{TP} was evaluated by HPLC. Briefly, 2.5 mg of MeNP₄^{TP} (containing 50 μ g TP) suspended in 1 mL of PBS containing 10% FBS was added to the dialysis bag (MWCO = 3500 Da). Then, the dialysis bag was immersed in a flask containing 200 mL of PBS and 0.5% SDS at 37 °C. 100 μ L of sample was taken at time points for TP analysis by HPLC.

4.6. Animals

Female C57BL/6J mice (4-6-weeks-old) were purchased from the Animal Experimental Center of Jilin University (Changchun, China) and kept under thermo-regulated, humidity-controlled conditions under a 12 h day/night light cycle provided by the experimental and were fed with standard rat chow and water ad libitum. All animal studies were carried out in Changchun Institute of Applied Chemistry, Chinese Academy of Sciences, and the operating procedures of the experimental animals were carried out in accordance with the protocols approved by the Committee for Animal Research of Changchun Institute of Applied Chemistry, Chinese Academy of Sciences China.

4.7. In vivo biodistribution

To establish AKI mice model, the C57BL/6J mice were intraperitoneally injected with cisplatin at 20 mg kg⁻¹. The AKI mice were intravenously injected with DiR-labeled MeNP₂, MeNP₄, MeNP₆ or free DiR (equivalent to 50 μ g DiR kg⁻¹, 5 mice per group) at 3 days post-injection of cisplatin. At 24 h post-injection, mice were euthanized and the major organs (heart, liver, spleen, lung and kidney) were collected for fluorescence imaging using the IVIS® Spectrum system (Caliper, Hopkinton, MA, USA).

4.8. Cell culture

HK-2 cells were cultured in Dulbecco's modified Eagle medium (DMEM) supplemented with 10% FBS, 100 units mL⁻¹ penicillin and 100 units mL⁻¹ streptomycin at 37 °C in humidified atmosphere with 5% CO₂. The medium was changed every other day.

4.9. Cell viability assessment

Cell viability was determined by MTT assay. 100 μ L of culture medium containing 1 \times 10⁴ HK-2 cells were plated in each well of a 96-well microplate for overnight growth. Then, the culture medium was replaced with 100 μ L of fresh medium containing various concentrations of TP, MeNP₄ or MeNP₄^{TP} (equivalent to 0–50 ng mL⁻¹ TP or 0–2.5 μ g mL⁻¹ MeNP₄). After 24 h of incubation, the medium was replaced with 100 μ L of fresh medium containing 20 μ L of 5 mg mL⁻¹ MTT solution. After 3.5 h of incubation in the dark, each well was added

150 μL of DMSO and the absorbance was measured at 490 nm by microplate reader.

4.10. Cell protection from oxidative stress injury

1.5×10^5 HK-2 cells were cultured in 24-well plate overnight. Then, the cell medium was changed with fresh medium containing cisplatin (1 mg mL^{-1}) or cisplatin (1 mg mL^{-1}) with TP, MeNP₄ or MeNP₄^{TP} (equivalent to 20 ng mL^{-1} TP or $1 \mu\text{g mL}^{-1}$ MeNP₄) for 24 h. The fresh medium without cisplatin was used as control group. For cellular ROS and RNS detection, the treated cells were washed three times by PBS, and incubated with $10 \mu\text{mol L}^{-1}$ of H2DCFDA or R21 fluorescent probe at 37°C for 30 min, and analyzed by Shimadzu UV-3600 spectrophotometer. For the apoptotic/necrotic cell analysis, the treated cells were collected, centrifuged at 1000 rpm for 5 min and washed three times with PBS. Cells were suspended in PBS and stained with $5 \mu\text{L}$ of $100 \mu\text{g mL}^{-1}$ PI and $5 \mu\text{L}$ of $100 \mu\text{g mL}^{-1}$ Annexin-FITC, and analyzed by flow cytometry.

4.11. Cellular uptake

1.5×10^5 HK-2 cells were seeded in 24-well plate overnight, and then incubated with $1 \mu\text{g mL}^{-1}$ RhB-labeled MeNP₄ or MeNP₄^{TP} for 3 h. Then, the cells were washed with PBS three times. Cell uptake of MeNP₄ or MeNP₄^{TP} in HK-2 cells was determined by flow cytometry (BD Biosciences, AccuriC6) and fluorescence microscopy (Zeiss Axio Vert A1, Germany).

4.12. Macrophage transformation, DC maturation and T cell activation

1.5×10^5 RAW 264.7 cells were seeded in 24-well plate for 12 h growth, and then pretreated with LPS (100 ng mL^{-1}) for 24 h to obtain M1 phenotype, followed by treatment with TP, MeNP₄ or MeNP₄^{TP} (equivalent to 20 ng mL^{-1} TP or $1 \mu\text{g mL}^{-1}$ MeNP₄) for another 24 h and further incubated with different antibodies: anti-F4/80-FITC ($1 \mu\text{g mL}^{-1}$, clone BM8, Biolegend), anti-CD206-APC ($1 \mu\text{g mL}^{-1}$, clone C068C2, Biolegend), and anti-CD86-PE ($1 \mu\text{g mL}^{-1}$, clone GL-1, Biolegend) for 30 min. Flow cytometry (BD Biosciences, AccuriC6) was applied to analyze the expression of CD206 and CD86 on RAW 264.7 cells. And the supernatant was centrifuged at 3000 rpm for 10 min to remove cell debris or dead cell, and the TNF- α and IL-10 levels were assessed by ELISA kit (Biolegend) according to manufacturer's instruction.

1.5×10^5 immature DCs separated from the bone marrow cells of normal C57BL/6J mice were seeded in 24-well plate, and then pretreated with LPS (100 ng mL^{-1}) for 24 h to induced DCs maturation, followed by treatment with TP, MeNP₄ or MeNP₄^{TP} (equivalent to 20 ng mL^{-1} TP or $1 \mu\text{g mL}^{-1}$ MeNP₄) for another 24 h and further incubated with different antibodies: anti-CD80-FITC ($1 \mu\text{g mL}^{-1}$, clone BM8, Biolegend) and anti-CD86-PE ($1 \mu\text{g mL}^{-1}$, clone GL-1, Biolegend) for 30 min. Flow cytometer (BD Biosciences, AccuriC6) was applied to analyze the expression of CD80 and CD86 on DC.

5.0×10^4 spleen cells separated from the spleen of normal C57BL/6J mice were seeded in 24-well plate, and then treated with TP, MeNP₄ or MeNP₄^{TP} (equivalent to 20 ng mL^{-1} TP or $1 \mu\text{g mL}^{-1}$ MeNP₄) in the presence of CD3/CD28 ($5 \mu\text{g mL}^{-1}$) for 48 h. Then, spleen cells were collected for detection of T cells activation by flow cytometer (BD Biosciences, AccuriC6) through staining with anti-CD4-PE ($1 \mu\text{g mL}^{-1}$, clone GK1.5, Biolegend) and anti-FOXP3-APC ($1 \mu\text{g mL}^{-1}$, clone 53-6.7, Biolegend) for 30 min.

4.13. In vivo therapeutic evaluation

At 3 h after the cisplatin injection, the AKI mice were intravenously injected with PBS, TP, MeNP₄ or MeNP₄^{TP} (equivalent to 0.01 mg kg^{-1} TP or 0.5 mg kg^{-1} of MeNP₄) for 3 consecutive days, respectively. Blood

samples, urine samples and renal tissue were harvested after 3 days of the treatment. Blood was withdrawn retroorbitally and allowed to clot for 4 h. The serum was separated by centrifugation at 3000 rpm. The BUN and CREA in the serum were detected using the standard kits (Nanjing Institute of Biological Engineering, China) according to the manufacturer's protocol. Kim-1 and Ngal in the serum and urine were detected using the standard kits (Jianglai Biotechnology, Shanghai, China) according to the manufacturer's protocol. And the renal tissues were sectioned, and stained with H&E, and subsequently studied by a fluorescence microscopy (Zeiss Axio Vert A1, Germany) to evaluate the therapeutic effect of MeNP₄^{TP} *in vivo*. In addition, the major organs (including heart, liver, spleen and lung) of the treated mice were also collected, sectioned and stained by H&E. The images were captured by a fluorescence microscopy (Zeiss Axio Vert A1, Germany) to evaluate the toxicity of MeNP₄^{TP} *in vivo*.

4.14. In vivo RONS scavenging and inflammation alleviation

For RONS scavenging detection in the kidneys, the above treated mice were sacrificed to harvest kidneys after 3 days of the treatment. 50 mg of fresh renal tissue was made into homogenate with 1 mL of tissue lysate, followed by 10 min of centrifugation at 12000 rpm at 4°C . Then, 190 μL of the supernatant was collected and incubated with 10 μL of DCF ROS probe (BestBio, China) or O52 RNS probe (BestBio, China) in one well of a 96-well plate at 37°C in the dark for 30 min. Fluorescence intensity that reflects the ROS or RNS level was quantified by fluorescence microplate reader (Bio-Tek Instruments, USA).

For inflammation alleviation detection in the kidneys, the above treated mice were sacrificed to harvest kidneys after 3 days of the treatment, and the single cell suspension of the kidneys was prepared and stained with anti-F4/80-FITC ($1 \mu\text{g mL}^{-1}$, clone BM8, Biolegend), anti-CD206-APC ($1 \mu\text{g mL}^{-1}$, clone C068C2, Biolegend), and anti-CD86-PE ($1 \mu\text{g mL}^{-1}$, clone GL-1, Biolegend) for 30 min, respectively, to detect the percentage of M1 and M2 phenotype macrophages, or stained with anti-FOXP3-APC ($1 \mu\text{g mL}^{-1}$, clone 53-6.7, Biolegend) and anti-CD4-PE ($1 \mu\text{g mL}^{-1}$, 30 min, clone GK1.5, Biolegend) for 30 min, respectively, to detect the percentage of CD4⁺T cells and Treg cells (CD4⁺FOXP3⁺), or stained with anti-CD80-FITC ($1 \mu\text{g mL}^{-1}$, clone 16-10A1, Biolegend) and anti-CD86-PE ($1 \mu\text{g mL}^{-1}$, clone GL-1, Biolegend) for 30 min, respectively, to detect the DC maturation by flow cytometer (BD Biosciences, AccuriC6 and FACSCanto II). The serum of the above treated mice was collected to examine the levels of IFN- γ , IL-1 β , TNF- α and IL-10 using ELISA kit (Biolegend) according to manufacturer's instruction.

4.15. Survival analysis

For survival studies, at 3 h after the cisplatin injection, the AKI mice were divided into 4 groups (PBS, TP, MeNP₄ or MeNP₄^{TP}) with 10 mice in each group. Then, the AKI mice were intravenously injected with PBS, TP, MeNP₄ or MeNP₄^{TP} (equivalent to 0.01 mg kg^{-1} TP or 0.5 mg kg^{-1} MeNP₄) for consecutive 3 days. The treated mice were followed for up to 10 days monitoring survival after the cisplatin injection.

4.16. Statistical analysis

All data analyses were performed using GraphPad Prism 6.0 (GraphPad Software, La Jolla, CA, USA). Data are presented as the mean \pm SD. Student's t-test was used to analyze differences between two groups. One-way ANOVA was used to perform the multi-sample analysis followed by the Tukey post hoc test. Differences at $p < 0.05$ were considered statistically significant (* $p < 0.05$; ** $p < 0.01$; *** $p < 0.001$; ns, not significant).

Declarations

Ethics approval and consent to participate. The Committee for

Animal Research of Changchun Institute of Applied Chemistry, Chinese Academy of Sciences China approved all animal experiments

Funding

This work was supported by National Key Research and Development Program of China (2021YFE0100300, 2021YFF0704805), National Natural Science Foundation of China (82102193, 22077119, 22007087), Science and Technology Development Plan Project of Jilin Province (20220101047JC, 20200201516JC).

CRedit authorship contribution statement

Xiaoqing Han: Writing – original draft, Visualization, Methodology, Investigation, Funding acquisition, Formal analysis, Data curation, Conceptualization. **Luopeng Bi:** Data curation. **Jiao Yan:** Data curation. **Panpan Song:** Data curation. **Yanjing Wang:** Data curation. **Xingbo Wang:** Data curation. **Yunyun Wu:** Data curation. **Xiaobo Ding:** Visualization. **Haiyuan Zhang:** Supervision, Validation, Writing – review & editing. **Yanbo Wang:** Supervision. **Xi Li:** Supervision.

Declaration of competing interest

The authors declare that they have no known competing financial interests or personal relationships that could have appeared to influence the work reported in this paper.

Data availability

Data will be made available on request.

Appendix A. Supplementary data

Supplementary data to this article can be found online at <https://doi.org/10.1016/j.mtbio.2024.101002>.

References

- J.A. Kellum, J.R. Prowle, Paradigms of acute kidney injury in the intensive care setting, *Nat. Rev. Nephrol.* 14 (2018) 217–230.
- M.S. Oh, Evaluation of renal function, water, electrolytes, and acid-base Balance, in: R.A. McPherson, M.R. Pincus (Eds.), *Henry's Clinical Diagnosis and Management by Laboratory Methods*, 22 Ed., W.B. Saunders, Philadelphia, 2011, pp. 169–192.
- L.S. Chawla, P.W. Eggers, R.A. Star, P.L. Kimmel, Acute kidney injury and chronic kidney disease as interconnected syndromes, *N. Engl. J. Med.* 371 (2014) 58–66.
- G.M. Chertow, E. Burdick, M. Honour, J.V. Bonventre, D.W. Bates, Acute kidney injury, mortality, length of stay, and costs in hospitalized patients, *J. Am. Soc. Nephrol.* 16 (2005) 3365–3370.
- R. Bellomo, J.A. Kellum, C. Ronco, R. Wald, J. Martensson, M. Maiden, S. M. Bagshaw, N.J. Glassford, Y. Lankadeva, S.T. Vaara, A. Schneider, Acute kidney injury in sepsis, *Intensive Care Med.* 43 (2017) 816–828.
- A. Khwaja, KDIGO clinical practice guidelines for acute kidney injury, *Nephron Clin. Pract.* 120 (2012) c179–c184.
- Z. Liu, L. Xie, K. Qiu, X. Liao, T.W. Rees, Z. Zhao, L. Ji, H. Chao, An ultrasmall RuO₂ nanozyme exhibiting multienzyme-like activity for the prevention of acute kidney injury, *ACS Appl. Mater. Interfaces* 12 (2020) 31205–31216.
- K.A. Nath, S.M. Norby, Reactive oxygen species and acute renal failure, *Am. J. Med.* 109 (2000) 665–678.
- K. Hosohata, Role of oxidative stress in drug-induced kidney injury, *Int. J. Mol. Sci.* 17 (2016) 1826.
- J.M. Dennis, P.K. Witting, Protective pole for antioxidants in acute kidney disease, *Nutrients* 9 (2017) 718.
- G. Ramesh, W.B. Reeves, Inflammatory cytokines in acute renal failure, *Kidney Int. Suppl.* (2004) S56–S61.
- L. Zheng, W. Gao, C. Hu, C. Yang, R. Rong, Immune cells in ischemic acute kidney injury, *Curr. Protein Pept. Sci.* 20 (2019) 770–776.
- S.A. Lee, S. Noel, M. Sadasivam, A.R.A. Hamad, H. Rabb, Role of immune cells in acute kidney injury and repair, *Nephron* 137 (2017) 282–286.
- J. Gong, S. Noel, J. Hsu, E.L. Bush, L.J. Arend, M. Sadasivam, S.A. Lee, J. T. Kurzhagen, A.R. A Hamad, H. Rabb, TCR+CD4–CD8– (double negative) T cells protect from cisplatin-induced renal epithelial cell apoptosis and acute kidney injury, *Am. J. Physiol. Ren. Physiol.* 318 (2020) F1500–F1512.
- B. Zheng, G. Deng, J. Zheng, Y. Li, B. Wang, X. Ding, W. Xue, P. Tian, C. Ding, Self-polymerized polydopamine-based nanoparticles for acute kidney injury treatment through inhibiting oxidative damages and inflammatory, *Int. J. Biochem. Cell Biol.* 143 (2022) 106141.
- Y. Lu, Z. Gu, Kidney physiology: a size bandpass filter, *Nat. Nanotechnol.* 12 (2017) 1023–1025.
- B. Du, X. Jiang, A. Das, Q. Zhou, M. Yu, R. Jin, J. Zheng, Glomerular barrier behaves as an atomically precise bandpass filter in a sub-nanometre regime, *Nat. Nanotechnol.* 12 (2017) 1096–1102.
- M. Yu, J. Xu, J. Zheng, Renal clearable luminescent gold nanoparticles: from the bench to the clinic, *Angew. Chem. Int. Ed.* 58 (2019) 4112–4128.
- H. Kang, J. Gravier, K. Bao, H. Wada, J.H. Lee, Y. Baek, G.E. Fakhri, S. Gioux, B. P. Rubin, J. Coll, H.S. Choi, Renal clearable organic nanocarriers for bioimaging and drug delivery, *Adv. Mater.* 28 (2016) 8162–8168.
- M. Yu, C. Zhou, L. Liu, S. Zhang, S. Sun, J.D. Hankins, X. Sun, J. Zheng, Interactions of Renal-clearable gold nanoparticles with tumor microenvironments: vasculature and acidity effects, *Angew. Chem. Int. Edn. Engl.* 56 (2017) 4314–4319.
- B. Du, M. Yu, J. Zheng, Transport and interactions of nanoparticles in the kidneys, *Nat. Rev. Mater.* 3 (2018) 358–374.
- R. Nielsen, E.I. Christensen, H. Birn, Megalin and cubilin in proximal tubule protein reabsorption: from experimental models to human disease, *Kidney Intern* 89 (2016) 58–67.
- J. He, H. Chen, W. Zhou, M. Chen, Y. Yao, Z. Zhang, N. Tan, Kidney targeted delivery of asiatic acid using a FITC labeled renal tubular-targeting peptide modified PLGA-PEG system, *Intern. J. Pharm.* 584 (2020) 119455.
- R.M. Williams, J. Shah, B.D. Ng, D.R. Minton, L.J. Gudas, C.Y. Park, D.A. Heller, Mesoscale nanoparticles selectively target the renal proximal tubule epithelium, *Nano Lett.* 15 (2015) 2358–2364.
- G. Zhong, X. Yang, X. Jiang, A. Kumar, H. Long, J. Xie, L. Zheng, J. Zhao, Dopamine-melanin nanoparticles scavenge reactive oxygen and nitrogen species and activate autophagy for osteoarthritis therapy, *Nanoscale* 11 (2019) 11605–11616.
- D.R. Amin, C. Sugnaux, K.H.A. Lau, P.B. Messersmith, Size control and fluorescence labeling of polydopamine melanin-Mimetic nanoparticles for intracellular imaging, *Biomimetics* 2 (2017) 17.
- Y. Lu, Y. Zhang, L. Li, X. Feng, S. Ding, W. Zheng, J. Li, P. Shen, TAB1: a target of triptolide in macrophages, *Chem. Biol.* 21 (2014) 246–256.
- G. Zhang, Y. Liu, H. Guo, Z. Sun, Yi Zhou, Triptolide promotes generation of FoxP3 + T regulatory cells in rats, *J. Ethnopharmacol.* 125 (2009) 41–46.
- H. Xu, H. Zhao, C. Lu, Q. Qiu, G. Wang, J. Huang, M. Guo, B. Guo, Y. Tan, C. Xiao, Triptolide inhibits osteoclast differentiation and bone resorption in vitro via enhancing the production of IL-10 and TGF- β 1 by regulatory T cells, *Mediators Inflamm* 2016 (2016) 8048170.
- K. Zhu, Q. Shen, H. Cheng, X. Mao, L. Lao, G. Hao, Triptolide affects the differentiation, maturation and function of human dendritic cells, *Int Immunopharmacol* 5 (2005) 1415–1426.
- R. Batul, M. Bhave, P.J. Mahon, A. Yu, Polydopamine nanosphere with in-Situ loaded gentamicin and its antimicrobial activity, *Molecules* 25 (2020) 2090.
- S.J. Holditch, C.N. Brown, A.M. Lombardi, K.N. Nguyen, C.L. Edelstein, Recent advances in models, mechanisms, biomarkers, and interventions in cisplatin-induced acute kidney injury, *Int. J. Mol. Sci.* 20 (2019) 3011.
- X. Deng, T. Zeng, J. Li, C. Huang, M. Yu, X. Wang, L. Tan, M. Zhang, A. Li, J. Hu, Kidney-targeted triptolide-encapsulated mesoscale nanoparticles for high-efficiency treatment of kidney injury, *Biomater. Sci.* 7 (2019) 5312.
- B. Poinard, S.A.E. Lam, K.G. Neoh, J.C.Y. Kah, Mucopenetration and biocompatibility of polydopamine surfaces for delivery in an Ex Vivo porcine bladder, *J Control Release* 300 (2019) 161–173.
- A. Zuk, J.V. Bonventre, Acute kidney injury, *Annu. Rev. Med.* 67 (2016) 293–307.
- A. Bonavia, K. Singbartl, A review of the role of immune cells in acute kidney injury, *Pediatr. Nephrol.* 33 (2018) 1629–1639.
- N. Song, T. Zhang, X. Xu, Z. Lu, X. Yu, Y. Fang, J. Hu, P. Jia, J. Teng, X. Ding, MiR-21 protects against ischemia/reperfusion-induced acute kidney injury by preventing epithelial cell apoptosis and inhibiting dendritic cell maturation, *Front. Physiol.* 9 (2018) 790.
- M.N. Martina, S. Noel, S. Bandapalle, A.R.A. Hamad, H. Rabb, T lymphocytes and acute kidney injury: update, *Nephron Clin. Pract.* 127 (2014) 51–55.
- S.M. Oh, G. Park, S.H. Lee, C.S. Seo, H.K. Shin, D.S. Oh, Assessing the recovery from prerenal and renal acute kidney injury after treatment with single herbal medicine via activity of the biomarkers HMGB1, NGAL and KIM-1 in kidney proximal tubular cells treated by cisplatin with different doses and exposure times, *BMC Complement Altern Med* 17 (2017) 544.